Editors' Suggestion

Towards supersensitive optical phase measurement using a deterministic source of entangled multiphoton states

G. Peniakov, Z.-E. Su, A. Beck, D. Cogan, O. Amar, and D. Gershoni*

The Physics Department and the Solid State Institute, Technion-Israel Institute of Technology, 3200003 Haifa, Israel

(Received 28 February 2020; revised manuscript received 5 May 2020; accepted 6 May 2020; published 3 June 2020)

Precision measurements of optical phases have many applications in science and technology. Entangled multiphoton states have been suggested for performing such measurements with precision that significantly surpasses the shot-noise limit. Until recently, such states have been generated mainly using spontaneous parametric down-conversion—a process which is intrinsically probabilistic, counteracting the advantages that the entangled photon states might have. Here we use a semiconductor quantum dot to generate entangled multiphoton states in a deterministic manner, using periodic timed excitation of a confined spin. This way we entangle photons one by one at a rate which exceeds 300 MHz. We use the resulting multiphoton state to demonstrate super-resolved optical phase measurement. Our results open up a scalable way for realizing genuine quantum enhanced supersensitive measurements in the near future.

DOI: 10.1103/PhysRevB.101.245406

I. INTRODUCTION

When a light beam passes through a thin layer of transparent material, it gains a phase shift relative to the same beam in vacuum. The shift depends, in general, on the thickness of the layer, its refractive index, and its birefringence. Measuring the optical phase has, therefore, numerous applications in science and technology, including microscopy, lithography, and displacement measurements, to name a few.

The precision in which such measurements can be performed is typically limited to the shot-noise-limit (SNL) of $\Delta\theta_{\mathrm{clas}} = 1/\sqrt{N}$, where N is the total number of the detected beam photons. A possible way to overcome this limit is to use entangled multiphoton states, which can conceptually push the measurement precision toward the Heisenberg limit of $1/N$ [1–3].

A well-known example is the N00N state [4,5]. Such a state of N_{ent} photons can be expressed as $(|N_{\mathrm{ent}}, 0\rangle + |0, N_{\mathrm{ent}}\rangle)/\sqrt{2}$, representing a superposition of all N_{ent} photons in one mode or all in another mode, with a well-defined quantum mechanical phase between the two. If one mode experiences a phase shift of θ relative to the other by passing a medium, then the entangled multiphoton state transfers to $(|N_{\mathrm{ent}}, 0\rangle + e^{iN_{\mathrm{ent}}\theta}|0, N_{\mathrm{ent}}\rangle)/\sqrt{2}$. The gained phase of $N_{\mathrm{ent}}\theta$ can be accurately measured using interferometry, for example, yielding a measure of θ with an error of $\Delta\theta_{\mathrm{ent}} = 1/N_{\mathrm{ent}}$. Since only a single mode emerging from a single source experiences the phase shift, the N00N states also provide high spatial resolution when measuring local phase shifts [6]. Unfortunately, generating a N00N state is a very demanding and resource-intensive task, and thus only N00N states with $N_{\mathrm{ent}} = 5$ photons have been reported so far [7].

The Greenberger-Horne-Zeilinger (GHZ) [8] state is yet another multiphoton entangled state that can be used for supersensitive phase measurements. It is expressed as $(|0\rangle^{\otimes N_{\mathrm{ent}}} + e^{i\alpha}|1\rangle^{\otimes N_{\mathrm{ent}}})/\sqrt{2}$, describing a superposition of N_{ent} photons, all in state $|0\rangle$ or all in state $|1\rangle$, with a well-defined relative phase α between the two cases. Similarly to the N00N case, if one of the states experiences a phase shift of θ relative to the other, then θ can, in principle, be measured in the Heisenberg accuracy limit.

In this work, we produce such a GHZ state where $|0\rangle$ and $|1\rangle$ are implemented in two orthogonal polarizations of the photons. GHZ states have already been produced with up to 12 [9] and 18 photonic qubits [10] using spontaneous parametric down-converted (SPDC) light sources [11]. Nevertheless, these sources are probabilistic, and require inefficient postselection in order to create the GHZ states. In addition, the spatial resolution that such GHZ states can provide is relatively limited. This is because the generated GHZ states occupy multiple spatial modes. These and other requirements challenge the use of SPDC sources as suitable and scalable sources for supersensitive phase measurement applications.

Single photon sources with spontaneously generated entanglement were also considered recently for achieving supersensitivity [12]. Single photon sources based on semiconductor quantum dots (QDs) are particularly bright and capable of deterministic production of single [13–15] and entangled [16–21] photons. Attempts to demonstrate phase supersensitive measurements were recently reported using entangled two-photon ($N_{\mathrm{ent}} = 2$) states from a single QD [22,23]. Unfortunately, these methods are intrinsically limited to low numbers of entangled photons [24,25].

Here we demonstrate an approach for achieving supersensitive optical phase measurement. This approach utilizes semiconductor QDs to deterministically generate multiphoton, polarization-entangled GHZ states. We do it by periodic pulsed excitation of the QD, entangling photons at a rate of 330 MHz. The number of photons that can be entangled (N_{ent}) in this way is in principle unlimited. In addition, the produced GHZ states occupy one spatial mode, providing the

*dg@physics.technion.ac.il

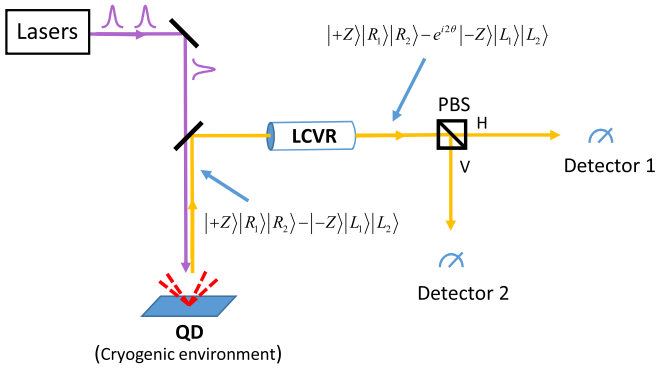

FIG. 1. Schematic and simplified description of the experimental system. A sequence of pulses is applied to the quantum dot (QD) at 76 MHz. The pulses deterministically generate a string of photons, which are polarization entangled with the spin of the dark exciton (DE) in the QD. The emitted photons pass through a liquid crystal variable retarder (LCVR), which adds adjustable relative phase difference between the two components of the light circular polarizations R and L. The polarization of the photons is then projected on two rectilinear polarizations H and V using a polarizing beam splitter (PBS). Correlation events in which two or three clicks occur during the same period are recorded by the time-tagging electronics.

highest spatial resolution possible. These advantages pave the way for building a scalable method for performing supersensitive measurements. We describe below the experiment that demonstrates the concept and discuss the conditions for achieving genuine supersensitivity.

II. THEORETICAL BACKGROUND

A. Optical phase measurement with classical light

Consider the experimental setup described in Fig. 1. We set a liquid crystal variable retarder (LCVR) to add a relative phase of θ between left- and right-circularly polarized light transmitted through the LCVRs. For example, rectilinear horizontally polarized light $|H\rangle = (|R\rangle + |L\rangle)/\sqrt{2}$ accumulates a phase of θ on transmission through the LCVR to become $(|R\rangle + e^{i\theta}|L\rangle)/\sqrt{2}$. A way to measure the accumulated phase θ is to project the light on a polarizing beam splitter (PBS). One measures then the degree of rectilinear polarization at the output, which is given by $D_{\rm RP}(\theta) = \frac{I_H(\theta)-I_V(\theta)}{I_H(\theta)+I_V(\theta)}$, where $I_H(\theta)$ [$I_V(\theta)$] is the intensity of the light transmitted (reflected) by the PBS. It is straightforward to show that

$$\begin{aligned} I_{H(V)}(\theta) &\propto \tfrac{1}{2}[1 \pm D_{\rm RP}(\theta)] \\ D_{\rm RP}(\theta) &= D^{\rm S}_{\rm RP}\cos(\theta), \end{aligned} \tag{1}$$

where $D^{\rm S}_{\rm RP}$ is the degree of rectilinear polarization of the light source before the LCVR (ideally $D^{\rm S}_{\rm RP} = 1$).

The best uncertainty in determining θ, $\Delta\theta$ is therefore given by:

$$\begin{aligned} \Delta\theta &= \frac{\Delta D_{\rm RP}}{\partial D_{\rm RP}(\theta)/\partial\theta} \\ &= \frac{\Delta D_{\rm RP}}{D^{S}_{\rm RP}|\partial\cos(\theta)/\partial\theta|_{\cos(\theta)=0}} = \frac{\Delta D_{\rm RP}}{D^{\rm S}_{\rm RP}}, \end{aligned} \tag{2}$$

where one chooses the angle θ such that $D_{\rm RP}(\theta)$ almost vanishes, and its slope maximizes. Here $\Delta D_{\rm RP}$ is the experimental uncertainty in measuring the degree of rectilinear polarization after the LCVR, for θ close to such a point ($\theta \simeq \pi/2$). For classical light this uncertainty is given precisely by $1/\sqrt{N}$, where N is the total number of photons used for measuring $D_{\rm RP}$. It follows that $\Delta\theta_{\rm clas} = \frac{1}{D^{\rm S}_{\rm RP}\sqrt{N}}$.

B. Optical phase measurement with entangled light

For nonclassical light composed of $N/N_{\rm ent}$ bunches of $N_{\rm ent}$ entangled photons in each bunch, forming a GHZ state, $(|R\rangle^{\otimes N_{\rm ent}} + |L\rangle^{\otimes N_{\rm ent}})/\sqrt{2}$, the considerations are slightly different. This time, transmission through the LCVR results in accumulated phase of $N_{\rm ent}\theta$ between the left and right polarization components $(|R\rangle^{\otimes N_{\rm ent}} + e^{iN_{\rm ent}\theta}|L\rangle^{\otimes N_{\rm ent}})/\sqrt{2}$. Measuring the degree of rectilinear polarization in this case allows the determination of θ with higher accuracy. To see this, one obtains, as before [see Eq. (2)],

$$\begin{aligned} I^{N_{\rm ent}}_{H(V)}(\theta) &\propto \tfrac{1}{2}\left[1 \pm D^{N_{\rm ent}}_{\rm RP}(\theta)\right] \\ D^{N_{\rm ent}}_{\rm RP}(\theta) &= D^{{\rm S},N_{\rm ent}}_{\rm RP}\cos(N_{\rm ent}\theta), \end{aligned} \tag{3}$$

where $D^{{\rm S},N_{\rm ent}}_{\rm RP}$ is the degree of rectilinear polarization of the entangled light source. Substituting this in the expression for $\Delta\theta$, recalling that in this case the uncertainty in the measured polarization degree is given by the number of bunches: $\Delta D^{N_{\rm ent}}_{\rm RP} = (N/N_{\rm ent})^{-\frac{1}{2}}$ yields

$$\begin{aligned} \Delta\theta_{N_{\rm ent}} &= \frac{\Delta D^{N_{\rm ent}}_{\rm RP}}{D^{{\rm S},N_{\rm ent}}_{\rm RP}|\partial\cos(N_{\rm ent}\theta)/\partial\theta|_{\cos(N_{\rm ent}\theta)=0}} \\ &= \frac{1}{D^{{\rm S},N_{\rm ent}}_{\rm RP}\sqrt{N}\sqrt{N_{\rm ent}}} = \frac{\Delta\theta_{\rm clas}}{\sqrt{N_{\rm ent}}}, \end{aligned} \tag{4}$$

which means that if the initial degree of rectilinear polarization $D^{{\rm S},N_{\rm ent}}_{\rm RP}$ of the entangled light is the same as that of the classical light ($D^{{\rm S},N_{\rm ent}}_{\rm RP} = D^{\rm S}_{\rm RP} = D^{{\rm S},1}_{\rm RP}$) and if all N photons are detected, the sensitivity of the optical phase measurement with entangled light is $\sqrt{N_{\rm ent}}$ times better than that of the classical light.

Equation (4) holds for the ideal case in which each bunch of $N_{\rm ent}$ photons is maximally entangled and the efficiency of the photon detection, η, is 1. In reality, however, the situation is different [26,27]. The system detection efficiency is limited, and therefore for a finite η, the efficiency of detecting $N_{\rm ent}$-photon events is given by $\eta^{N_{\rm ent}}$. This means that in order to reach genuine supersensitivity even with entangled light of only $N_{\rm ent} = 2$, η should exceed 0.71. For supersensitivity which is order of magnitude better than the classical limit, $N_{\rm ent}$ should be more than 100 and η should be better than 98%.

Another obstacle in reaching genuine supersensitivity is the deviation of the multiphoton entangled state from a pure state. Typically, due to various decoherence processes in the state generation, adding photons to the multiphoton state results in greater coherence loss. This loss can often be described by a characteristic exponential decay in the degree of rectilinear polarization $D^{{\rm S},N_{\rm ent}}_{\rm RP}$ of the entangled light source, as the number of entangled photons $N_{\rm ent}$ increases:

$$D^{{\rm S},N_{\rm ent}}_{\rm RP} = D^{{\rm S},1}_{\rm RP}\, e^{-(N_{\rm ent}-1)/N_{\rm D}}, \tag{5}$$

where $D_{\mathrm{RP}}^{\mathrm{S},1}$ is the degree of rectilinear polarization of the classical light beam composed of single nonentangled photons and N_{D} is a characteristic polarization decay length of the entangled photon string.

With this dependence, although the increase in the string length improves the sensitivity as $\sqrt{N_{\mathrm{ent}}}$, at the same time the exponential decay of the D_{RP} reduces it. For the ideal case in which $D_{\mathrm{RP}}^{\mathrm{S},1} = 1$ and $\eta = 1$ it is straightforward to show that for a given N_{D} maximum sensitivity is obtained when $N_{\mathrm{ent}} = N_{\mathrm{D}}/2$. With this at hand, it follows that supersensitivity which is about 10% better than the SNL can be achieved with $N_{\mathrm{ent}} = 2$ entangled photons from an entangled light source with $N_{\mathrm{D}} \geqslant 4$. In order to get supersensitivity which is an order of magnitude better than the SNL, bunches longer than $N_{\mathrm{ent}} = 270$ entangled photons are required from a light source with $N_{\mathrm{D}} \geqslant 540$. The limit in which $N_{\mathrm{D}} \to \infty$, $D_{\mathrm{RP}}^{\mathrm{S},1} = 1$, and $\eta = 1$ is called the Heisenberg limit.

III. EXPERIMENT

A. The dark exciton as a photon entangler

We use a QD to implement a scheme for deterministic generation of a string of entangled photons [28]. A QD-confined dark exciton (DE) forms a physical two-level system, effectively acting as a matter spin qubit (Fig. 2) [29]. Its two total spin (2) projections on the QD symmetry axis $\hat{z}$ form a basis, $|\pm Z\rangle = |\pm 2\rangle$, for the DE qubit space. The DE energy eigenstates are $|\pm X\rangle = (|+Z\rangle \pm |-Z\rangle)/\sqrt{2}$, with an energy splitting $\Delta\varepsilon_2 = 1.5\ \mu$eV. In the Bloch sphere representation, this splitting corresponds to a coherent state precession around the $\hat{x}$ axis, with a period of $T_{\mathrm{DE}} = h/\Delta\varepsilon_2 \backsimeq 3$ ns [29]. In addition to the DE, we use two states of a biexciton (BIE), a bound state of two excitons whose total spin projections on the spatial $\hat{z}$ axis are either $+3$ or -3. The BIE eigenstates $|\pm X_{\mathrm{BIE}}\rangle = (|+Z_{\mathrm{BIE}}\rangle \pm |-Z_{\mathrm{BIE}}\rangle)/\sqrt{2}$ are also nondegenerate, having precession period of $T_{\mathrm{BIE}} = h/\Delta\varepsilon_3 \backsimeq 5$ ns [30]. We denote these states by $|\pm 3\rangle$. The experimental protocol relies on the optical transition rules $|+2\rangle \longleftrightarrow |+3\rangle$ and $|-2\rangle \longleftrightarrow |-3\rangle$ through right-hand $|R\rangle$ and left-hand $|L\rangle$ circularly polarized photons, respectively (see Fig. 2).

The pulse sequence for generating the $|\mathrm{GHZ}\rangle$ state is schematically described by the energy-levels diagram in the lower panel of Fig. 3. It is executed at a rate of 76 MHz, corresponding to a time window of ~13 ns. Within each time window, a $|\mathrm{GHZ}\rangle$ state is generated and used for the optical phase measurement.

First, we deterministically initialize the DE in its spin eigenstate $|\psi_{\mathrm{DE}}^{\mathrm{init}}\rangle = |-X\rangle = (|+2\rangle - |-2\rangle)/\sqrt{2}$ using a short π-area picosecond pulse [29,31]. The pulse is tuned to an absorption resonance of the DE, which acquires non-negligible oscillator strength due to residual mixing with the bright exciton [32]. After the initialization, we repeatedly apply a cycle containing three elements: (i) a converting laser π pulse, resonantly tuned to the DE-BIE optical transition [29]; (ii) subsequent radiative recombination of the BIE, resulting in an emission of a photon entangled with the spin of the DE which remains confined in the QD [28]; and (iii) timed free precession of the DE spin for one full period [33]. In the first step of the cycle (i), the pulse is horizontally polarized

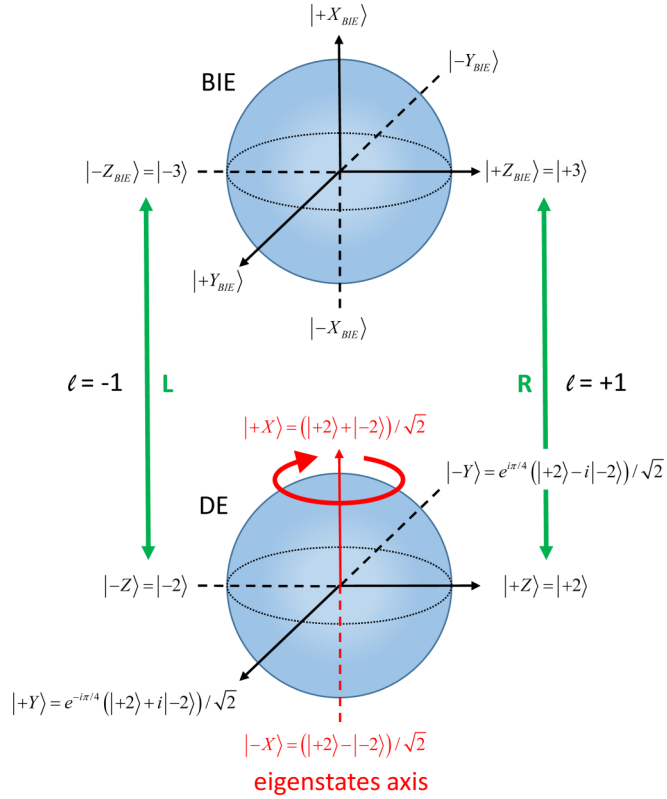

FIG. 2. The Bloch spheres describing the dark exciton (DE) spin two level system and the biexciton (BIE). The degeneracy of the qubits two eigenstates $|\pm X\rangle$ is lifted by the exchange interaction leading to precession around the $\hat{x}$ axis of any coherent superposition of the qubit's eigenstates. The circularly polarized optical transitions which connects between the two qubits are marked by the green vertical arrows.

$|H\rangle = (|R\rangle + |L\rangle)/\sqrt{2}$—an equal superposition of right- and left-hand circular polarizations. It converts the DE state into the BIE state: $|\psi_{\mathrm{BIE}}\rangle = (|+3\rangle - |-3\rangle)/\sqrt{2}$, keeping the same relative phase between the $\pm$ spin state components. In step (ii), radiative recombination of this BIE results in an entangled state of the DE spin and the emitted photon polarization $\sqrt{2}|\psi_{\mathrm{DE\text{-}1ph}}\rangle = (|Z\rangle|R_1\rangle - |-Z\rangle|L_1\rangle)$. In step (iii), the DE completes full rotation around the Bloch $\hat{x}$ axis, thus returning to its original state after the BIE decays:

$$|+Z\rangle \to |+Y\rangle \to |-Z\rangle \to |-Y\rangle \to |+Z\rangle \qquad (6)$$

where we subdivided the evolution into increments of quarters of precession period.

The sequence of steps (i) and (ii) forms one full cycle. Repeating the cycle again results in a second photon, whose polarization state is entangled with that of the first photon and the spin of the remaining DE, yielding the tripartite GHZ state:

$$\sqrt{2}\,|\psi_{\mathrm{DE\text{-}1ph\text{-}2ph}}\rangle = (|Z\rangle|R_1\rangle|R_2\rangle - |-Z\rangle|L_1\rangle|L_2\rangle). \qquad (7)$$

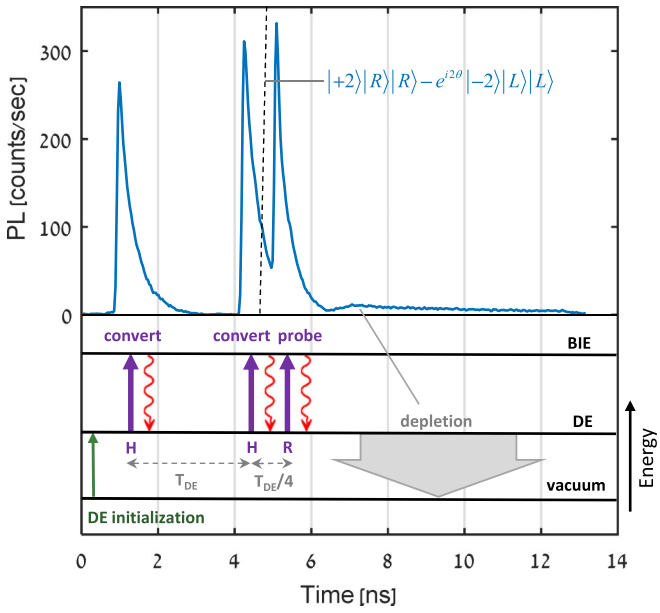

FIG. 3. Time-resolved photoluminscence (PL) signal (upper panel) and the 76-MHz pulse sequence for generating the entangled GHZ state (lower panel). Within 13 ns the DE is initialized [31] (green upward arrow), converted $N_{\text{ent}} = 2$ times to the BIE level using rectilinearly polarized π pulses (purple arrows), and separated apart by the DE precession time [29]. As a result, $N_{\text{ent}} = 2$ photons are emitted represented in the figure by the curly downward red arrows. The emitted photons pass the LCVR and then their polarizations are projected on the rectilinear basis by the PBS as shown in Fig. 1. The last pulse is circularly polarized, and timed quarter of a precession after the previous pulse. The detection of the resulted emitted photon projects the DE spin on the $|Y\rangle$ basis. The emitted photons are detected by single photon detectors, as shown by the time resolved trace in the upper panel. Detection of three-photon events during one period forms a projection of the multiqubit $|\psi(\theta)_{\text{DE-1ph-2ph}}\rangle$ GHZ state. The sequence ends with a few-nanoseconds depletion pulse [34], which removes the DE from the QD and prepares the QD for the next period.

In terms of the pulse sequence (Fig. 3), this state is generated with the emission of the second BIE photon following the second converting pulse.

This cycle can be applied N_{ent} times to generate an entangled $N_{\text{ent}} + 1$ GHZ state, containing N_{ent} photons and a DE.

$$\sqrt{2}\,|\psi_{\text{DE-1ph-2ph-}\ldots\text{-}N_{\text{ent}}}\rangle = |Z\rangle|R_1\rangle|R_2\rangle\ldots|R_{N_{\text{ent}}}\rangle - |-Z\rangle|L_1\rangle|L_2\rangle\ldots|L_{N_{\text{ent}}}\rangle. \quad (8)$$

When the emitted photons pass through the retarder of Fig. 1, the state evolves to:

$$\sqrt{2}\,|\psi_{\text{DE-1ph-2ph-}\ldots\text{-}N_{\text{ent}}}\rangle = |Z\rangle|R_1\rangle|R_2\rangle\ldots|R_{N_{\text{ent}}}\rangle - e^{iN_{\text{ent}}\theta}|-Z\rangle|L_1\rangle|L_2\rangle\ldots|L_{N_{\text{ent}}}\rangle. \quad (9)$$

The last pulse is circularly polarized. It excites the DE quarter of a precession period after the previous pulse. Detecting the emitted photon after this pulse projects the DE state on the $|Y\rangle$ basis. The cycle then ends in a ~7-ns-long optical pulse, which depletes the QD and prepares it for the next cycle [34].

B. Calculating the multiqubit quantum state using the repeated cycle's process map

The multiqubit states that our method produces deviate from the pure wave functions $\psi(\theta)_{\text{DE-1ph}}$ and $\psi(\theta)_{\text{DE-1ph-2ph-...Nent}}$, described above. The proper way to describe our actual output state is within the formalism of density matrices. We can calculate the density matrix of the multiqubit state that we produce by applying repeatedly a linear transformation Φ to the initial state of the DE. The transformation Φ is called a "process map" and it describes the evolution of the system from N_{ent} qubits to $N_{\text{ent}} + 1$ [28]. For example, one can describe the evolution of any initial DE state (spanned by a 2×2 density matrix) when it is subjected to the excitation, photon emission, and full periodic precession of the DE, resulting in an entangled DE-photon state (spanned by a 4×4 density matrix), by:

$$\rho_{\alpha\beta}^{(\text{DE+1ph})} = \sum_{\mu} \Phi_{\alpha\beta}^{\mu} \rho_{\mu}^{(\text{DE})}. \quad (10)$$

Here the density matrix elements are given in the Pauli basis, such that $\hat{\rho}^{(\text{DE})} = \sum_{\mu} \rho_{\mu}^{(\text{DE})} \hat{\sigma}_{\mu}$, $\hat{\rho}^{(\text{DE+1ph})} = \sum_{\alpha\beta} \rho_{\alpha\beta}^{(\text{DE+1ph})} \hat{\sigma}_{\alpha} \otimes \hat{\sigma}_{\beta}$, where $\mu, \alpha, \beta \in 0, 1, 2, 3$. The process map has, therefore, 64 real parameters. To measure the process map, we first perform full tomography of the initialized DE in six different initialization states $|\pm X\rangle, |\pm Y\rangle, |\pm Z\rangle$ [35]. Next, we apply to these states one cycle of our protocol and perform full two-qubit tomography on the resulting entangled DE-photon states. Finally, by solving a set of linear equations, the process map Φ is fully obtained [28]. The fidelity of our measured map to the ideal one, which describes an ideal two-qubit gate and no decoherence at all, is 0.82.

Having the process map at hand, we apply it N_{ent} times to the measured initialization of the DE state, simulating the resulting $(N_{\text{ent}} + 1)$ GHZ state. Then we add a phase of $\cos(N_{\text{ent}}\theta)$ to the $|L\rangle\langle L|$ component of the density matrix relative to the $|R\rangle\langle R|$ one, imitating the action of the LCVRs on the transmitted photons. Finally, we project the simulated $N_{\text{ent}} + 1$ qubits density matrix on the orthogonal basis elements (photons on $|\pm X\rangle$ and spin on $|\pm Y\rangle$), as done in the experiment.

C. Experimental system

A simplified version of the experimental system appears in Fig. 1. A sequence of laser pulses is launched on the QD, resulting in emission of a string of single photons separated from each other by ~3 ns. The photons are polarization entangled as explained above. By passing through the LCVR an optical phase of θ is added to $|L\rangle$ polarized photons relative to the $|R\rangle$ polarized ones. Here we used the setup to produce $N_{\text{ent}} = 1$ and $N_{\text{ent}} = 2$ entangled spin-photon and entangled spin-photon-photon ($|\text{GHZ}\rangle$) states, respectively. The photons are then projected using a standard PBS and detected using superconducting single-photon detectors. In principle, one pair of detectors is enough to perform the demonstration, provided that their recovery time is shorter than the temporal separation of two sequential photons (3 ns). In practice, since the recovery time of our detectors is longer than that (~20 ns), we used two more detectors, allowing us to measure up to

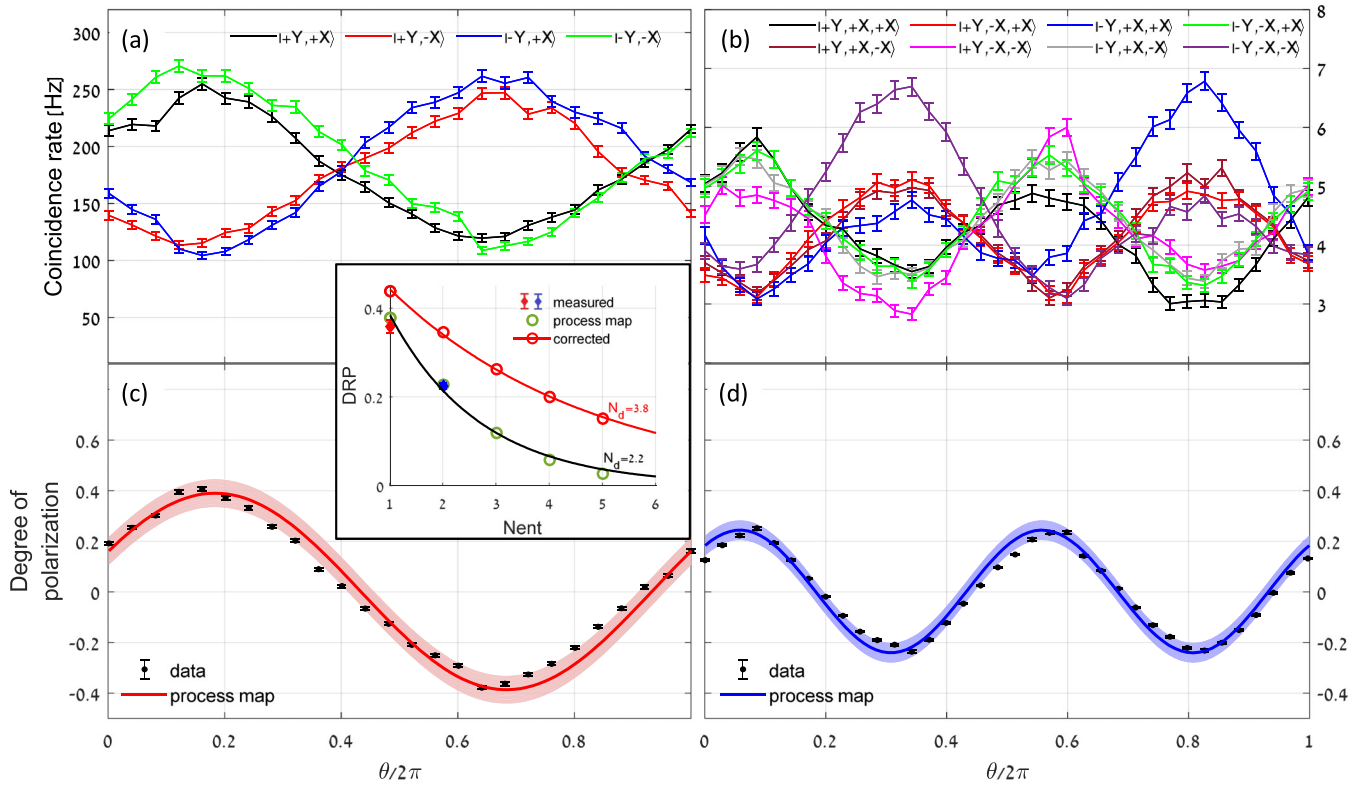

FIG. 4. Coincidence rates as a function of the LCVR phase θ. (a) Two-photon coincidence rate of all four $|\psi(\theta)_{\text{DE-1ph}}\rangle$ state projections. Note that two have a positive $\cos(\theta)$ dependence and two a negative $\cos(\theta)$ dependence [see Eq. (1)]. (b) Three-photon coincidence rates of all 8 $|\psi(\theta)_{\text{DE-1ph-2ph}}\rangle$ state projections. Like in (a), four have positive $\cos(2\theta)$ dependence and four have negative $\cos(2\theta)$ dependence [see Eq. (3)]. (c) Measured (symbols) and calculated (solid red line) degree of rectilinear polarization [$D^1_{\text{RP}}(\theta)$]. (d) Measured (symbols) and calculated (solid blue line) $D^2_{\text{RP}}(\theta)$. For the calculations of $D^1_{\text{RP}}(\theta)$ and $D^2_{\text{RP}}(\theta)$ we used the measured process map. The color-matched shaded areas represent the uncertainty in the calculations due to one standard deviation uncertainty in the measured process map. The inset describes the measured (symbols) and calculated from the process map (green circles) $D^{S,N_{\text{ent}}}_{\text{RP}}$. The black solid line describes characteristic exponential decay with $N_{\text{D}} = 2.2 \pm 0.2$, best fitted to measured and calculated by the process map $D^{S,N_{\text{ent}}}_{\text{RP}}$. The red solid line describes best fitted exponential decay with $N_{\text{D}} = 3.8 \pm 0.2$ to the calculated $D^{S,N_{\text{ent}}}_{\text{RP}}$ corrected for the depletion efficiency (red circles).

four-photon correlations. We used a HydraHarp time-tagging device to record two- and three-photon coincidence events for projection-measurements of the $N_{\text{ent}} = 1$ and $N_{\text{ent}} = 2$ cases, respectively. We recorded the coincidence rates while scanning θ between 0 and 2π. A coincidence event is registered whenever two (or three) photons are detected within the same repetition cycle of 13 ns. The overall collection efficiency of our system, is estimated as 1%, thereby resulting in three-photon coincidence rate of ∼150 Hz.

IV. RESULTS AND DISCUSSION

When a coincidence event is recorded, the data analysis proceeds as follows: The detection of the last photon which results from the last $|R\rangle$ ($|L\rangle$) circularly polarized excitation pulse is used to project the DE spin on the $|+Y_0\rangle$ ($|-Y_0\rangle$) base. The preceding pulse(s), which result from $|H\rangle$ polarized excitation pulse(s) are detected in either $|H\rangle$ or $|V\rangle$ polarization, thereby projecting the detected photons on either the $|+X\rangle$ or $|-X\rangle$ basis states.

For the case of spin-photon entanglement $|\psi(\theta)_{\text{DE-1ph}}\rangle$ two-photon correlation measurements are used. In Fig. 4(a), we present the measured coincidence rates as a function of θ for each one of the four possible projections. Two of them, $|+Y_0\rangle|+X_1\rangle$ and $|-Y_0\rangle|-X_1\rangle$, depend on θ through $A[1 + D^{\text{S},1}_{\text{RP}}\cos(\theta)]$, where A is the average two-photon coincidence rate [see Eqs. (1) and (2)]. We call this dependence a "positive $\cos(\theta)$" dependence, referring to the plus sign coefficient of $\cos(\theta)$. The other two projections, $|+Y_0\rangle|-X_1\rangle$ and $|-Y_0\rangle|+X_1\rangle$, have a "negative $\cos(\theta)$" dependence through $A[1 - D^{\text{S},1}_{\text{RP}}\cos(\theta)]$. Similarly, for the case of spin-photon-photon entanglement three-photon correlation measurements are used. We then project the three-qubit $|\text{GHZ}\rangle$ state, $|\psi(\theta)_{\text{DE-1ph-2ph}}\rangle$, on eight different possible polarization basis elements. Four of these projections, namely:

$$|+Y_0\rangle|+X_1\rangle|+X_2\rangle, \quad |+Y_0\rangle|-X_1\rangle|-X_2\rangle,$$
$$|-Y_0\rangle|-X_1\rangle|+X_2\rangle, \quad |-Y_0\rangle|+X_1\rangle|-X_2\rangle,$$

have positive $\cos(2\theta)$ dependence and four, obtained simply by flipping all the signs in the expressions above, have negative dependence [see Eq. (3)]. Figure 4(b) presents the rate of three-photon coincidences as a function of θ for all these eight projections.

The measured $D^{N_{\text{ent}}}_{\text{RP}}(\theta)$ for $N_{\text{ent}} = 1$ and 2 as deduced from Figs. 4(a) and 4(b) are given by the data points in Fig. 4(c) and in Fig. 4(d), respectively. As can be seen in these figures the measured data points are indeed well described by

functions of the form $D_{\mathrm{RP}}^{S,1}\cos(\theta)$ and $D_{\mathrm{RP}}^{S,2}\cos(2\theta)$, respectively, as presented in the figures by the calculated solid lines.

The observed frequency doubling in the three-photon correlation events as compared with the two-photon correlations is termed "super-resolution." It demonstrates the gain in the accuracy of the optical phase measurements, resulting from the use of the $N_{\mathrm{ent}}=2$ entangled photon state.

We note here that in principle, the function $D_{\mathrm{RP}}^{N_{\mathrm{ent}}}(\theta)$ can be measured directly by our system, without measuring first coincidence rates at various projections. This is because the sign dependence of the measured DRP in a given bunch of N_{ent} photons can be deduced directly from the measurement results. In each individual bunch measurement i, the degree of rectilinear polarization is given by $D_{\mathrm{RP}}^{i}=\frac{N_H^i-N_V^i}{N_H^i+N_V^i}$, where N_H^i (N_V^i) is the number of $|H\rangle$ ($|V\rangle$) polarized photons among the detected photons before the last detected one in a given bunch. ($N_H^i+N_V^i=N_{\mathrm{ent}}$ equals 1 (2) in Fig. 4(a) [Fig. 4(b)]). The sign of the $\cos(N_{\mathrm{ent}}\theta)$ dependence is given by the sign of the spin projection base $|\pm Y_0^i\rangle$ and the parity of the number of photons detected in $|V\rangle$ polarization. The measured degree of rectilinear polarization is therefore given by:

$$D_{\mathrm{RP}}=\sum_{i=1}^{N/N_{\mathrm{ent}}}\mathrm{sign}(|\pm Y_0^i\rangle)(-1)^{N_V^i}D_{\mathrm{RP}}^{i} \tag{11}$$

where N is the total number of photons in the experiment.

The inset in Fig. 4(c) presents the measured $D_{\mathrm{RP}}^{\mathrm{S},N_{\mathrm{ent}}}$ (diamond-shape marks) and calculated $D_{\mathrm{RP}}^{\mathrm{S},N_{\mathrm{ent}}}$ by the process map (circle-shape marks). Using the measured and calculated amplitudes in Eq. (5) one finds that the characteristic decay of the D_{RP} of our state is given by $N_{\mathrm{D}}=2.2\pm0.2$.

We note that the D_{RP} of the single photon beam that we produced, $D_{\mathrm{RP}}^{\mathrm{S},1}\backsimeq 0.4$, is relatively low. The reason for this is attributed to the limited efficiency ($\sim$75%) by which we deplete the QD before the DE preparation [34]. This inefficient depletion, can be measured directly by the PL emission intensity at the end of the depletion pulse (see Fig. 3). The limited depletion reduces both the fidelity of DE state preparation and the fidelity of the DE spin projection, resulting in the measured $D_{\mathrm{RP}}^{\mathrm{S},1}$ of 0.4 only. In fact, if one takes this inefficiency into account, corrects the initial state for it, and applies the process map on a fully depleted QD, then the characteristic DRP decay length becomes $N_{\mathrm{D}}=3.8\pm0.2$, as can be seen in the inset to Fig. 4(c). With this decay length genuine supersensitivity of a few percentages can be achieved with $N_{\mathrm{ent}}=2$ entangled photons (and $\eta\geqslant 0.71$).

To see this, we display in Fig. 5 the calculated enhancement of the optical phase resolution relative to the SNL, as a function of N_{ent}. We display it for several sources of varying quality, characterized by their DRP characteristic decay lengths, N_{D}. As can be seen in Fig. 5 for a given source quality, an optimum is obtained if the number of entangled photon used (N_{ent}) equals half of the characteristic decay length. Using this condition, we plot in the inset to Fig. 5 the enhancement in the optical phase measurement with respect to the SNL as a function of the number of entangled photons in a bunch under this condition ($N_{\mathrm{ent}}=N_D/2$). The few-percentages super-resolution that we achieved is represented by the data point in Fig. 5 and in its inset. The case in which all the photons in a given bunch are maximally entangled ($N_{\mathrm{D}}\rightarrow\infty$) is represented in the inset by a dashed line (Heisenberg limit).

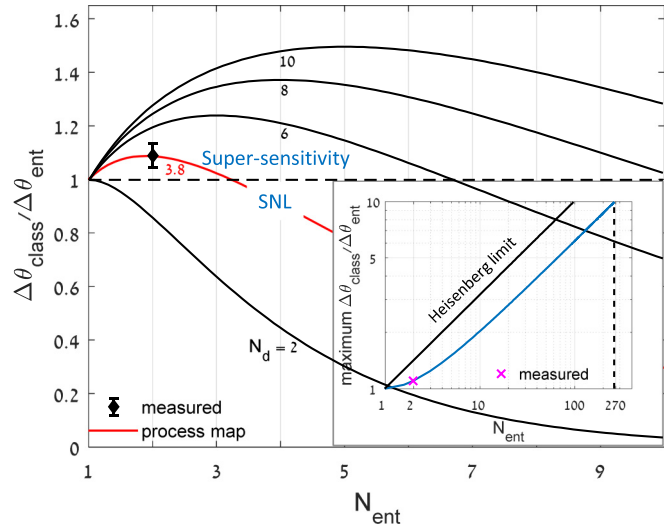

FIG. 5. The enhancement in the optical phase resolution relative to the SNL, as a function of the number of entangled photons bunch length N_{ent} for various characteristic decay length N_{D}. The red curve represents the performance of our device as deduced from its measured process map. The black diamonds indicate the measured points, normalized for ideal initialization of the DE. With better QD depletion, genuine supersensitivity of a few percents could be achieved. The inset shows maximum sensitivity enhancement as a function of $N_{\mathrm{ent}}=N_{\mathrm{D}}/2$. An order-of-magnitude better resolution requires bunches of $N_{\mathrm{ent}}=270$ entangled photons from a source quality of $N_{\mathrm{D}}=540$. The solid diagonal line represents the case in which $N_{\mathrm{D}}\rightarrow\infty$, for which the Heisenberg limit is obtained.

In summary, we have demonstrated a way for achieving supersensitivity in optical phase measurement using deteministically prepared entangled multiphoton GHZ state. We outlined the required conditions for achieving genuine supersensitivity and showed that there are no conceptual physical barriers which prevent achieving this long-desired technological goal.

ACKNOWLEDGMENTS

The support of the Israeli Science Foundation (ISF) and that of the European Research Council (ERC) under the European Union's Horizon 2020 research and innovation program (Grant No. 695188) are gratefully acknowledged.

[1] H. Lee, P. Kok, and J. Dowling, J. Mod. Opt. **49**, 2325 (2002).
[2] V. Giovannetti, S. Lloyd, and L. Maccone, Nat. Photon. **5**, 222 (2011).
[3] S. Daryanoosh, S. Slussarenko, D. W. Berry, H. M. Wiseman, and G. J. Pryde, Nat. Commun. **9**, 4606 (2018).

[4] A. N. Boto, P. Kok, D. S. Abrams, S. L. Braunstein, C. P. Williams, and J. P. Dowling, Phys. Rev. Lett. **85**, 2733 (2000).

[5] M. W. Mitchell, J. S. Lundeen, and A. M. Steinberg, Nature **429**, 161 (2004).

[6] J. P. Dowling, Contemp. Phys. **49**, 125 (2008).

[7] I. Afek, O. Ambar, and Y. Silberberg, Science **328**, 879 (2010).

[8] P. Walther, J.-W. Pan, M. Aspelmeyer, R. Ursin, S. Gasparoni, and A. Zeilinger, Nature **429**, 158 (2004).

[9] H.-S. Zhong, Y. Li, W. Li, L.-C. Peng, Z.-E. Su, Y. Hu, Y.-M. He, X. Ding, W. Zhang, H. Li, L. Zhang, Z. Wang, L. You, X.-L. Wang, X. Jiang, L. Li, Y.-A. Chen, N.-L. Liu, C.-Y. Lu, and J.-W. Pan, Phys. Rev. Lett. **121**, 250505 (2018).

[10] X.-L. Wang, Y.-H. Luo, H.-L. Huang, M.-C. Chen, Z.-E. Su, C. Liu, C. Chen, W. Li, Y.-Q. Fang, X. Jiang, J. Zhang, L. Li, N.-L. Liu, C.-Y. Lu, and J.-W. Pan, Phys. Rev. Lett. **120**, 260502 (2018).

[11] J.-W. Pan, Z.-B. Chen, C.-Y. Lu, H. Weinfurter, A. Zeilinger, and M. Zukowski, Rev. Mod. Phys. **84**, 777 (2012).

[12] K. R. Motes, J. P. Olson, E. J. Rabeaux, J. P. Dowling, S. J. Olson, and P. P. Rohde, Phys. Rev. Lett. **114**, 170802 (2015).

[13] E. Dekel, D. Gershoni, E. Ehrenfreund, J. M. Garcia, and P. M. Petroff, Phys. Rev. B **61**, 11009 (2000).

[14] N. Somaschi, V. Giesz, L. De Santis, J. C. Loredo, M. P. Almeida, G. Hornecker, S. L. Portalupi, T. Grange, C. Antón, J. Demory, C. Gómez, I. Sagnes, N. D. Lanzillotti-Kimura, A. Lemaítre, A. Auffeves, A. G. White, L. Lanco, and P. Senellart, Nat. Photon. **10**, 340 (2016).

[15] X. Ding, Y. He, Z.-C. Duan, N. Gregersen, M.-C. Chen, S. Unsleber, S. Maier, C. Schneider, M. Kamp, S. Höfling, C.-Y. Lu, and J.-W. Pan, Phys. Rev. Lett. **116**, 020401 (2016).

[16] N. Akopian, N. H. Lindner, E. Poem, Y. Berlatzky, J. Avron, D. Gershoni, B. D. Gerardot, and P. M. Petroff, Phys. Rev. Lett. **96**, 130501 (2006).

[17] R. J. Young, R. M. Stevenson, P. Atkinson, K. Cooper, D. A. Ritchie, and A. J. Shields, New J. Phys. **8**, 29 (2006).

[18] M. Müller, S. Bounouar, K. D. Jöns, M. Glässl, and P. Michler, Nat. Photon. **8**, 224 (2014).

[19] R. Winik, D. Cogan, Y. Don, I. Schwartz, L. Gantz, E. R. Schmidgall, N. Livneh, R. Rapaport, E. Buks, and D. Gershoni, Phys. Rev. B **95**, 235435 (2017).

[20] J. Liu, R. Su, Y. Wei, B. Yao, S. F. C. d. Silva, Y. Yu, J. Iles-Smith, K. Srinivasan, A. Rastelli, J. Li, and X. Wang, Nat. Nanotechnol. **14**, 586 (2019).

[21] H. Wang, H. Hu, T.-H. Chung, J. Qin, X. Yang, J.-P. Li, R.-Z. Liu, H.-S. Zhong, Y.-M. He, X. Ding, Y.-H. Deng, Q. Dai, Y.-H. Huo, S. Höfling, C.-Y. Lu, and J.-W. Pan, Phys. Rev. Lett. **122**, 113602 (2019).

[22] A. J. Bennett, J. P. Lee, D. J. P. Ellis, T. Meany, E. Murray, F. F. Floether, J. P. Griffths, I. Farrer, D. A. Ritchie, and A. J. Shields, Sci. Adv. **2**, e1501256 (2016).

[23] M. Müller, H. Vural, C. Schneider, A. Rastelli, O. G. Schmidt, S. Höfling, and P. Michler, Phys. Rev. Lett. **118**, 257402 (2017).

[24] J. P. Olson, K. R. Motes, P. M. Birchall, N. M. Studer, M. LaBorde, T. Moulder, P. P. Rohde, and J. P. Dowling, Phys. Rev. A **96**, 013810 (2017).

[25] Z.-E. Su, Y. Li, P. P. Rohde, H.-L. Huang, X.-L. Wang, L. Li, N.-L. Liu, J. P. Dowling, C.-Y. Lu, and J.-W. Pan, Phys. Rev. Lett. **119**, 080502 (2017).

[26] K. J. Resch, K. L. Pregnell, R. Prevedel, A. Gilchrist, G. J. Pryde, J. L. O'Brien, and A. G. White, Phys. Rev. Lett. **98**, 223601 (2007).

[27] T. Nagata, R. Okamoto, J. L. O'Brien, K. Sasaki, and S. Takeuchi, Science **316**, 726 (2007).

[28] I. Schwartz, D. Cogan, E. R. Schmidgall, Y. Don, L. Gantz, O. Kenneth, N. H. Lindner, and D. Gershoni, Science **354**, 434 (2016).

[29] I. Schwartz, E. R. Schmidgall, L. Gantz, D. Cogan, E. Bordo, Y. Don, M. Zielinski, and D. Gershoni, Phys. Rev. X **5**, 011009 (2015).

[30] D. Cogan, O. Kenneth, N. H. Lindner, G. Peniakov, C. Hopfmann, D. Dalacu, P. J. Poole, P. Hawrylak, and D. Gershoni, Phys. Rev. X **8**, 041050 (2018).

[31] I. Schwartz, D. Cogan, E. R. Schmidgall, L. Gantz, Y. Don, M. Zieliński, and D. Gershoni, Phys. Rev. B **92**, 201201(R) (2015).

[32] M. Zieliński, Y. Don, and D. Gershoni, Phys. Rev. B **91**, 085403 (2015).

[33] E. Poem, Y. Kodriano, C. Tradonsky, N. H. Lindner, B. D. Gerardot, P. M. Petroff, and D. Gershoni, Nat. Phys. **6**, 993 (2010).

[34] E. R. Schmidgall, I. Schwartz, D. Cogan, L. Gantz, T. Heindel, S. Reitzenstein, and D. Gershoni, Appl. Phys. Lett. **106**, 193101 (2015).

[35] D. Cogan, G. Peniakov, Z.-E. Su, and D. Gershoni, Phys. Rev. B **101**, 035424 (2020).